Visible-Band Chiroptical Meta-Devices with Phase-Change Adjusted Optical Chirality

Lu Zhang,[†] *Kun Gao,*[†] *Fanfan Lu,*[†] *Lei Xu,*[‡] *Mohsen Rahmani,*[‡] *Lixun Sun,*[†] *Feng Gao,*[‖] *Wending Zhang,*,*[†] *and Ting Mei,*,*[†]

[†]Key Laboratory of Light Field Manipulation and Information Acquisition, Ministry of Industry and Information Technology, Northwestern Polytechnical University, Xi'an 710129, China

[‡]Advanced Optics & Photonics Laboratory, Nottingham Trent University, Nottingham NG11 8NS, United Kingdom

[‖]MOE Key Laboratory of Weak-Light Nonlinear Photonics, Nankai University, Tianjin 300457

KEYWORDS: Chirality meta-device, Circular dichroism, Phase change material

ABSTRACT: Low-cost large-area chirality meta-devices (CMDs) with adjustable optical chirality is of great interest for polarization-sensitive imaging, stereoscopic display, enantioselectivity analysis and catalysis. Currently, CMDs with adjusted chiroptical responses in the mid-infrared to terahertz band have been demonstrated by exploiting photocarriers of silicon, pressure, phase-change of GSTs, etc., but are still absent in the visible band, which in turn limits the development of chiral nanophotonic devices. Herein, by employing a phase-change material (Sb_2S_3), we present a protocol for the fabrication of wafer-scale visible-band enantiomeric CMDs with handedness, spectral, and polarization adjustability. As measured by circular dichroism, the chirality signs of CMDs enantiomers can be adjusted with Sb_2S_3 from amorphous to crystalline, and the chirality

resonance wavelength can also be adjusted. Our results suggest a new type of meta-devices with adjustable chiroptical responses that may potentially enable a wide range of chirality nanophotonic applications including highly sensitive sensing and surface-enhanced nanospectroscopy.

INTRODUCTION

Chirality, which means that an object that cannot coincide with its mirror image, is a fundamental property of nature. Biological macromolecules, such as proteins, nucleic acids, enzymes, etc., are the basis of life activities and all have chirality. Organic small molecule drugs with chirality enable disease treatment through strict chirality matching and molecular recognition with macromolecules.[1] Therefore, chirality has been widely exploited in the fields of medicine and pharmacy.

Except for chiral molecules existing in nature, many chirality meta-devices (CMDs), with strong chiroptical response over a wide spectral range, have also been prepared and potentially applied in polarization-sensitive optical elements,[2] nonlinear imaging,[3,4] catalysis,[5] etc. In the early design of CMDs, their structure dimensions, material permittivity, geometry, etc. were fixed, so their electromagnetic resonance could not be adjusted, which in turn limits the application of these nanostructures in the fields of active devices, such as modulators and tunable filters.[6]

To date, several methods have been proposed to realize tunable CMDs. The handedness of the terahertz-waveband chirality metamolecules was switched by utilizing the photocarrier effect in silicon and vertical deformation of micro-electro-mechanical systems.[7, 8] The phase change material $Ge_3Sb_2Te_6$ (GST), with a large refractive index difference between amorphous and crystalline states, was exploited in an active plasmonic chirality metamaterial in the mid-infrared waveband.[9] Reconfigurable chiroptical response of the optical nano-kirigami at the near-infrared wavelengths was achieved with attractive electrostatic forces.[10] Desoxyribonucleic acid can be

used both as a construction material to organize plasmonic nanorods into plasmonic metamolecules and as fuel to drive metamolecules into distinct conformational states in the visible band.[11, 12] In addition, the nanospheres/nanorods with different components and shapes were arranged into special spatial distributions to achieve chirality regulation at visible wavelengths.[13-17] Nevertheless, the large-area adjustable enantiomeric CMDs in the visible band have not yet been realized.

In this work, we propose wafer-scale enantiomeric CMDs by employing a phase-change material Sb_2S_3 with adjustable chiroptical responses in the visible band. By transforming the Sb_2S_3 film from amorphous to crystalline, the circular dichroism measurements demonstrated a chirality intensity modulation of ~610 mdeg, a spectral adjustment range of ~150 nm, and chirality sign adjustment accompanied with the maximum chirality intensity modulation from 252 mdeg to -1140 mdeg around the wavelength of 730 nm. Furthermore, the optical rotatory dispersion examination denoted that the spectrally adjustable CMDs can rotate the electric vector of the linearly polarized light by ~±15°, revealing a practical and compact phase-changed indued polarization modulator for the visible band.

RESULTS AND DISCUSSION

Fabrication and evaluation of CMDs. As illustrated in Figure 1(a), the D- and L-handed CMDs were fabricated via inductively coupled plasma (ICP) etching with a template of self-assembled polystyrene nanosphere array and subsequent glancing angle deposition (GLAD).[18, 19] Details on the preparation process can be found in Supplementary Note 1. φ is the angle between Ag and Au films deposited on the surface of the silica nanocone array. $+\varphi$ and $-\varphi$ correspond to D- and L-handed CMDs, as depicted by the insets in the dashed blue and red boxes shown in Figure 1(a), respectively. Wafer-scale CMDs can be easily and cost-effectively fabricated by this

process. Figure 1(b) shows the optical photograph of a D-handed CMD on a 10 cm-diameter silica wafer. A scanning electron microscopy (SEM, FEI Verios-G4) image with an area of 120 μm×80 μm can be seen in Supplementary Figure S6. The silica nanocone array prepared using a self-assembled polystyrene nanosphere array has a long-range disordered arrangement,[19] but by adjusting the angle of the laterally deposited noble metal layer, the influence of local random lattice orientation can be eliminated, thereby significantly enhancing the chiroptical response.[20, 21]

Figures 1(c) and (d) show the high magnification SEM images of the D- and L-handed CMDs with φ=90° and -90°, respectively. The height and bottom diameter of each nanocone unit are 700 nm and 400 nm, respectively, and the distance between adjacent units is 800 nm. For testing the chiroptical responses of the D- and L-handed CMDs, the circular dichroism (CD) spectrum was examined,[22] which is the difference of absorbances under the left- and right-hand circularly-polarized light (CPL) irradiation as a function of wavelength. Furthermore, the CMDs can be fabricated at wafer scale with uniform surface morphology, which significantly facilitates the use of conventional CD spectrometers (Chirascan) for characterization. Figure 1(f) shows the CD spectra of the D- and L-handed CMDs (φ=90° and φ=-90°, respectively) for frontside and backside irradiations as sketched in Figure 1(e). Notably, the backside irradiation of the CMDs results in stronger chiroptical response. Thus, the subsequent measurements were carried out using backside irradiation. The SEM images, CD spectra and *g*-factors of the CMDs with φ=±120°, ±150° are depicted in Supplementary Figures S7, S8. Figure 1(g) presents the relationship between the CD intensity and φ (±90°, ±120°, ±150°) at three resonance wavelengths 350 nm, 600 nm, and 750 nm. Note that, increasing φ leads to weakened chiroptical response, but the chiral resonance wavelengths are not significantly altered.

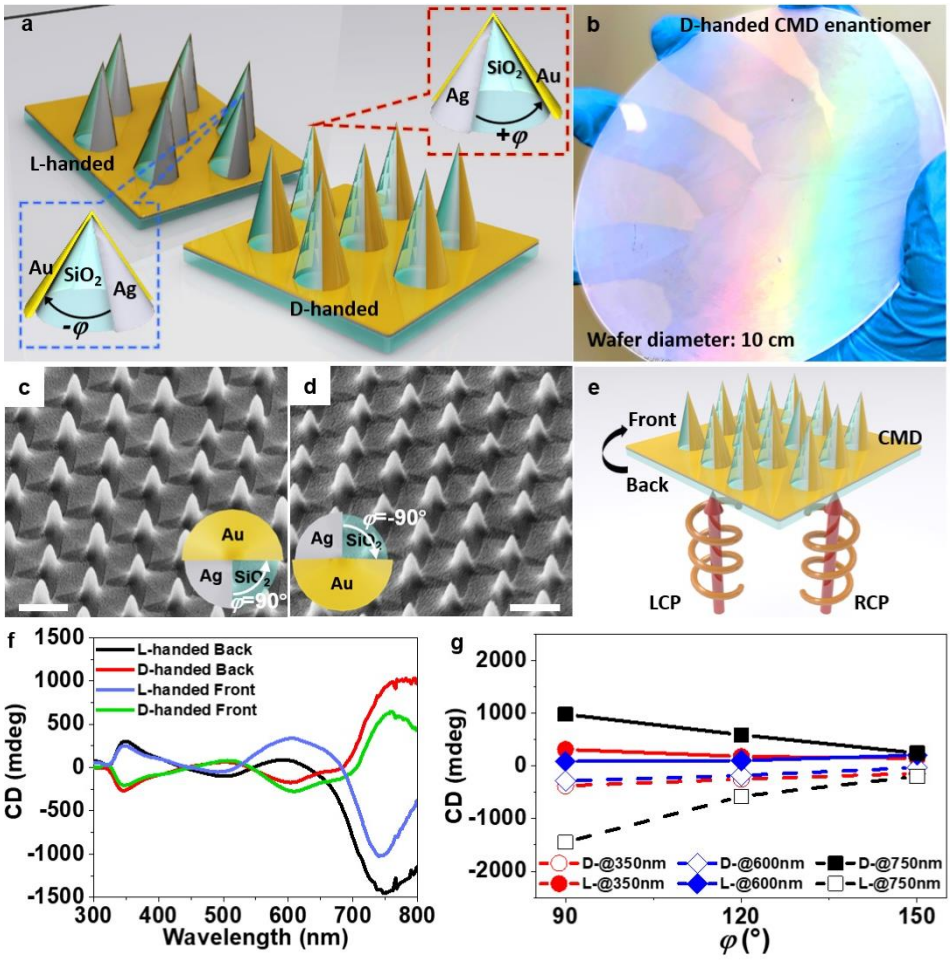

Figure 1. Morphology and CD measurement. (a) Schematic sketch of D- and L-handed CMDs. (b) Photograph of D-handed CMD with wafer diameter of 10 cm. SEM images of D- and L-handed CMDs with φ=90° (c) and -90° (d), respectively. Scale bars: 800 nm. (e) Sketch map of CD measurement. (f) CD spectra of D- and L-handed CMDs with a CPL wide-band light source illuminating the backside of D- (red curve) and L-handed (black curve) CMDs. Blue and green curves are CD spectra of D- and L-handed CMDs by illuminating the front side. (g) Relationship between CD intensity and φ at three wavelengths.

The chiroptical response was further interpreted by the 3D finite-difference time-domain (FDTD) method.[23] The structure parameters of CMDs were provided in Supplementary Note 1, and the details on the structure model of CMDs can be seen in Method. The calculated unpolarized

absorption spectra [Supplementary Figure S10] is coincided with the measurement results, indicating the rationality of the structural model. Figure 2(a) shows the calculated differential absorption cross-section spectra ($\Delta Abs = Abs_{LCP} - Abs_{RCP}$) of CMDs with $\varphi = \pm 90°$, where Abs_{LCP} and Abs_{RCP} are the absorption cross-section spectra under the left- and right-hand CPL [Supplementary Figure S11]. Note that the differential absorption cross-section spectra of the D- and L-handed CMDs present a bisignate feature, revealing mirror symmetry between these enantiomers.[24] The dissymmetry factor (*g*-factor) $g = \Delta Abs/A$ (A stands for unpolarized absorption of the CMDs) was estimated to be 0.07 at the wavelength of 750 nm, revealing excellent chiroptical responses of the CMDs.[25] In addition, the calculated differential absorption spectra for $\varphi = \pm 120°$, $\pm 150°$ are depicted in Supplementary Figure S12. The effect of φ on the chiroptical responses is theoretically investigated, as shown in Figure 2(b). At three major resonance wavelengths 329 nm, 516 nm, and 680 nm, all chiroptical responses are weakened by increasing φ, which is consistent with the experimental results shown in Figure 1(g).

The black curve in Figure 2(c) shows the calculated scattering spectrum of the D-handed CMD with $\varphi = 90°$, which has resonance peaks coincide with those in the differential absorption spectrum shown in Figure 2(a). A single CMD unit is a nanocone with graded diameter, thus exhibiting significant electromagnetic coupling properties at multiple wavelengths, which in turn exhibit multiple resonance peaks in the differential absorption spectrum. To simplify the theoretical analysis, we only picked up three major peaks at 329 nm, 516 nm, and 680 nm. They are mainly attributed to the electric quadrupole (EQ), magnetic dipole (MD), and electric dipole (ED), as seen from the multipole decomposition in Figure 2(c).[26] Furthermore, the enhanced optical chirality ($\left|C/C_{CPL}^{\pm}\right|$) of the D-handed CMD with $\varphi = 90°$ was calculated at two resonance

peaks of 516 nm and 329 nm. $C = -\varepsilon_0 \omega \mathrm{Im}\left(\mathbf{E}^* \cdot \mathbf{B}\right)/2c$ is the optical chirality distribution on the CMDs,[27] with **E** and **B** being of the complex electric and magnetic field amplitudes, respectively. $C_{CPL}^{\pm} = \pm\varepsilon_0 \omega |E|^2/2$ is the optical chirality of CPL in space, with "+" and "–" corresponding to the left- and right- handed CPL, respectively. The optical chirality distribution in *y*-*z* plane of the D-handed CMD at wavelengths of 329 nm and 516 nm are shown in Supplementary Figure S13. The D-handed CMD exhibits stronger chirality enhancement under right-handed CPL excitation than left-handed CPL excitation, agreement with the experimental results of CD spectra.

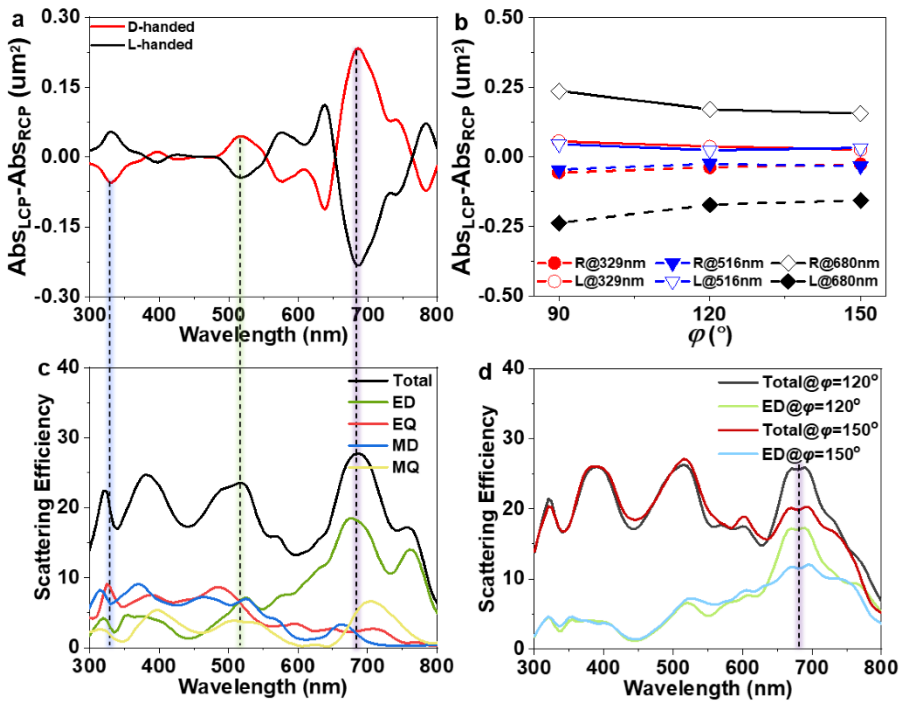

Figure 2. Theoretical calculations on CMDs. (a) Theoretically predicted ΔAbs of the D- and L-handed CMDs; (b) Relationship between ΔAbs and φ (±90°, ±120°, ±150°); (c) Calculated scattering spectra and multipole decomposition of the D-handed CMD with Mie theory. MD, magnetic dipole; ED, electric diploe; MQ, magnetic quadrupole; EQ, electric quadrupole. Calculated scattering spectra of the D-handed CMDs with φ=120° and 150°, and the corresponding multipole decomposition of ED mode.

The change of φ only affects the chirality intensities of the CMDs, but does not alter the resonance wavelengths. Multipole decomposition of the calculated scattering spectra of the D-handed CMD as shown Figure 2(d) indicates significant decrease of scattering efficiency near the resonance wavelength of 680 nm without shifting the ED resonance wavelength, as φ increases from 120° to 150°. The chiroptical response at 680 nm is still subject to the ED resonance, although its scattering efficiency decreases with increasing φ.

The electromagnetic mode resonance properties of the CMDs are sensitive to the surrounding dielectric environment. Therefore, by incorporating a Sb_2S_3 layer in the CMDs, the chiroptical response, including intensity, handedness and spectrum, can be adjusted via phase changing the Sb_2S_3 layer. Large refractive index difference $\Delta n \approx 1.26$ between the amorphous and crystalline Sb_2S_3 in the visible band can be well used to adjust the chiroptical response.[28] In addition, the nanocone arrays fabricated on silica wafers have not only excellent transmission efficiency in the visible band, but also excellent thermal and mechanical stability. Excellent surface morphology and uniformity can be maintained when thermal annealing is applied to phase change the Sb_2S_3 layer.

Adjustable optical chirality intensity of CMDs. As illustrated in Figures 3(a_1) and 3(b_1), a 50 nm Sb_2S_3 layer was deposited on the surface of the Ag film and silica nanocone. Then a 12 nm-thick silica layer was deposited on the Ag film and the Sb_2S_3 film surface to isolate the Sb_2S_3 film from the Ag and Au films to avoid interdiffusion between the metal and Sb_2S_3 films during the phase change process.[29] Furthermore, the Au film was deposited on the one-half surface of the Sb_2S_3 layer to form a pair of D- and L-handed CMDs, as shown in Figures 3(a_1) and 3(b_1). Lastly, a 12 nm-thick silica layer was deposited on the Au film and Sb_2S_3 layer to avoid island formation

of the Au film during the annealing process for crystallizing Sb_2S_3 [See Supplementary Figure S14]. The detailed preparation process of the CMDs is given in Supplementary Note 2.

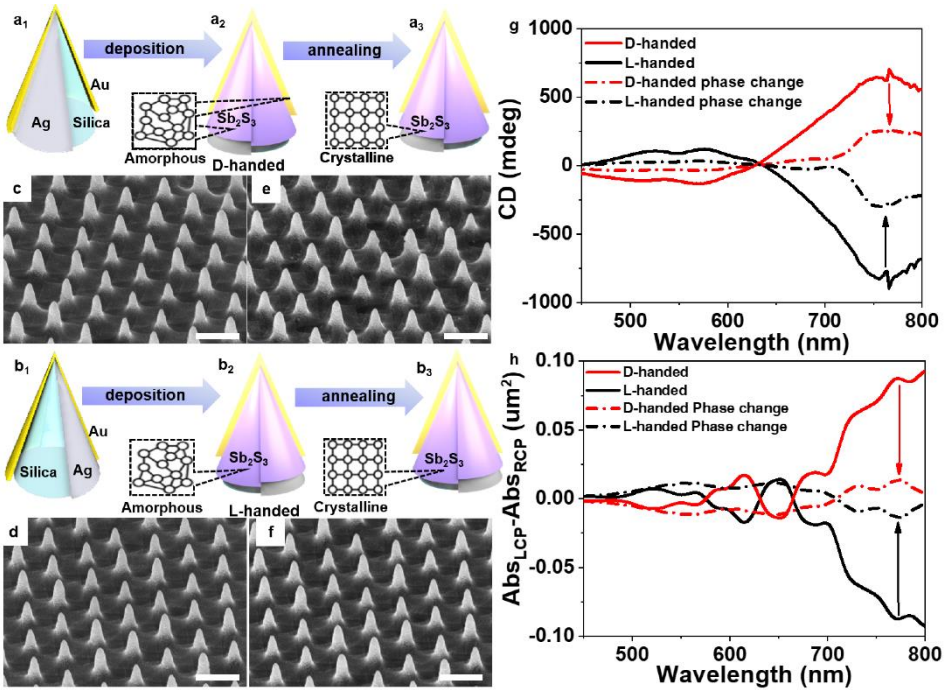

Figure 3. Chirality intensity adjustability of CMDs. Fabrication flowchart of D- (a_1-a_3) and L-handed (b_1-b_3) CMDs with chirality intensity adjustability. SEM images of D- and L-handed CMDs with amorphous (c, d) and crystalline (e, f) of Sb_2S_3 layer. Scale bars: 800 nm. Experimented CD (g) and simulated differential absorption (h) spectra of D- and L-handed CMDs with amorphous and crystalline of Sb_2S_3 layer.

Figures 3(c) and 3(d) show the SEM images of the D- and L-handed CMDs with an amorphous Sb_2S_3 layer, respectively. The chiroptical response is shown as the solid curves in Figure 3(g). In order to thermally transform the as-deposited amorphous Sb_2S_3 layer to the crystalline, the pair of CMDs enantiomers were heated simultaneously for 10 min at 275 °C under nitrogen atmosphere,[28] as respectively shown in Figures 3(a_3) and 3(b_3). Figures 3(e) and 3(f) are the SEM images of the D- and L-handed CMDs with crystalline Sb_2S_3 layer, revealing that the annealed CMDs still have a smooth surface. As shown in Figure 3(g), by transforming the

amorphous Sb_2S_3 layer to crystalline, the CD intensities at 760 nm changed from 718 mdeg to 262 mdeg for the D-handed CMD, and from -900 mdeg to -290 mdeg for the L-handed CMD, respectively, implying that a maximum chirality intensity modulation of ~610 mdeg was achieved by the phase change of Sb_2S_3. In FDTD simulation results shown in Figure 3(h) [Calculation details see Supplementary Figure S15], the differential absorption spectra are drastically changed at around 760 nm, which also indicates the chirality intensity adjustability enabled by the phase change of Sb_2S_3.

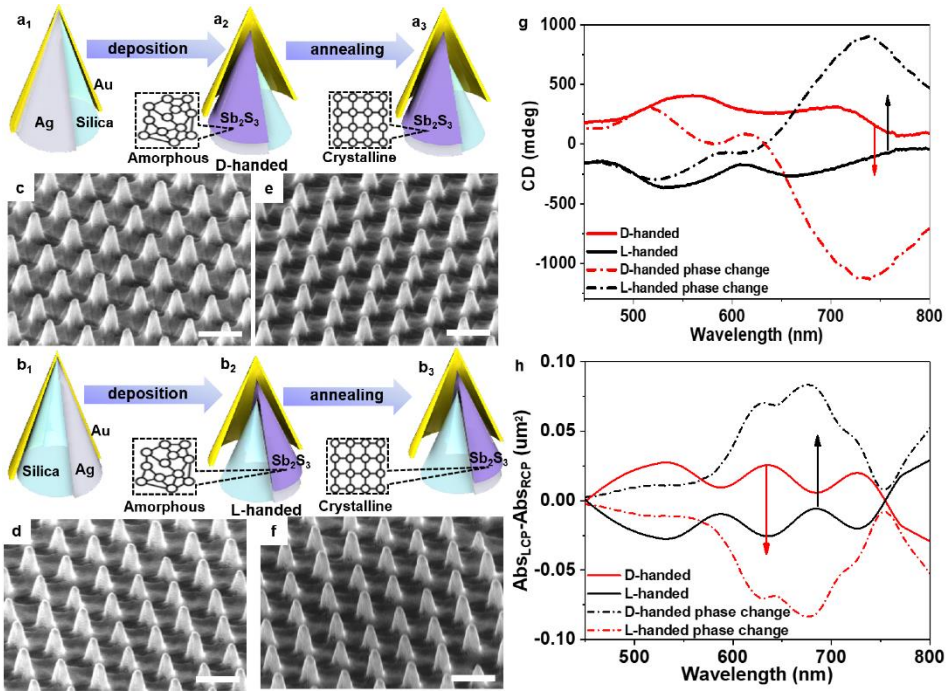

Figure 4. Adjustable chirality sign of CMDs. Fabrication flowchart of the D- (a_1-a_3) and L-handed (b_1-b_3) CMDs with function of chirality sign adjustment. SEM images of the D- and L-handed CMDs with amorphous (c, d) and crystalline (e, f) state of the phase change layer. Scale bars: 800 nm. Experimented CD (g) and simulated differential absorption (h) spectra of the D- and L-handed CMDs with amorphous and crystalline of Sb_2S_3 layer.

Adjustable chirality sign of CMDs. As illustrated in Figures. 4(a_1-a_2) and 4(b_1-b_2), a 50 nm-thick Sb_2S_3 layer was coated only on the surface of the Ag film, then a 12 nm-thick silica layer

was deposited on the Ag film and the silica nanocone surface, simultaneously. The Au film was deposited on the one-half surface of the silica film. Lastly, a 12 nm-thick silica layer was deposited on the Au film surface. The detailed preparation process is given in Supplementary Note 3.

Figures 4(c) and 4(d) show the SEM images of the D- and L-handed CMDs with an amorphous Sb_2S_3 layer, respectively, and the chiroptical responses are plotted as the solid curves in Figure 4(g). In addition, Figures 4(e) and 4(f) show the SEM images of the D- and L-handed CMDs with the Sb_2S_3 layer transformed to the crystalline, and the corresponding chiroptical responses are plotted as the dashed black and red curves in Figure 4(g), respectively. By phase changing Sb_2S_3 to the crystalline, the CD intensity of the L-handed CMD increased from -159 mdeg to 873 mdeg near the wavelength of 730 nm, and the CD intensity of D-handed CMD decreased from 252 mdeg to -1140 mdeg near the wavelength of 730 nm. Notably, the signs of the CD signals were adjusted to the opposite. The adjustment of chirality sign of CMDs was also examined by numerical simulation, as shown in Figure 4(h). The simulation agrees to the experimental results of optical chirality sign adjustment and chiroptical response enhancement via phase change of Sb_2S_3, except a blue-shift of the calculated differential absorption spectra, possibly due to deviation of the FDTD model from the real structure.

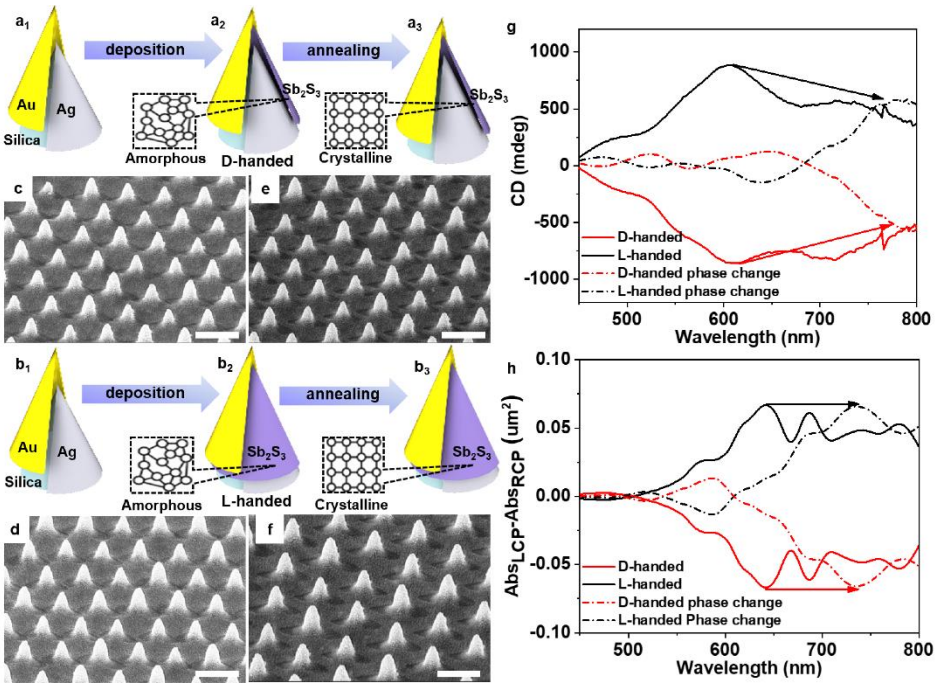

Figure 5. Spectrum adjustability of CMDs. Fabrication flowchart of D- (a_1-a_3) and L-handed (b_1-b_3) CMDs with spectral adjustability. SEM images of CMDs with amorphous (c, d) and crystalline (e, f) of Sb_2S_3 layer. Scale bars: 800 nm. Experimented CD and simulated differential absorption spectra of CMDs with amorphous (g) and crystalline (h) of Sb_2S_3 layer.

Spectrum adjustability of CMDs. The spectrum adjustable CMDs can also be fabricated with a film deposition strategy as illustrated in Figures. 5(a_1) and 5(b_1). A 50 nm-thick Sb_2S_3 film was simultaneously deposited on the half surface of the Ag film and the silica nanocone instead of deposited on the Ag film surface only. Next, a 12 nm-thick silica layer was deposited on the entire nanocone surface. Lastly, an Au film was deposited on the one-half surface of the silica film to complete the CMDs. The detailed preparation process is given in Supplementary Note 4. Figures 5(c) and 5(d) show the SEM images of the D- and L-handed CMDs, respectively, and the corresponding chiroptical responses are shown as the solid curves in Figure 5(g). Likewise, annealing was used to transform the Sb_2S_3 layer to the crystalline, as illustrated in Figures. 5(a_3) and 5(b_3). Figures 5(e) and 5(f) show the SEM images of the D- and L-handed CMDs with

crystallized Sb_2S_3 layer, and the corresponding chiroptical responses are shown as the dashed black and red curves in Figure 5(g), respectively. As the Sb_2S_3 film was changed from amorphous to crystalline, the resonance wavelength of the D- and L-handed CMDs has been shifted from 600 nm to 750 nm. The phase change of Sb_2S_3 lead to a wavelength shift up to ~27%. The spectral adjustability of the D- and L-handed CMDs was theoretically examined, as shown in Figure 5(h). The simulation results show that the resonance wavelength of the CMDs was shifted from 640 nm to 740 nm, corresponding to a 20% wavelength shift. Furthermore, the optical activity of spectrum tunable CMDs was characterized by optical rotation dispersion (ORD), which was the spectrum of the polarization rotation angle (θ) arising from the transmission-phase difference between the two circular polarizations. When the Sb_2S_3 layer was changed from amorphous to crystalline, θ was changed significantly within the spectral range of 450 nm-800 nm, and the maximum θ is ±15° at 780 nm. The details of ORD examination and simulation can be found in Supplementary Note 5.

CONCLUSION

Summary, we presented the visible-band CMDs with optical chirality adjusted by phase-changing Sb_2S_3. CMDs with wafer scale have been fabricated via a process of self-assembly, ICP etching followed by GLAD. Quantitative analysis of CD reveals excellent chiroptical responses in the visible band, with a maximum dissymmetry factor of ~0.07. Furthermore, by designing a film deposition strategy with a Sb_2S_3 layer, the intensity, handedness, and spectrum of CMDs can be adjusted through the Sb_2S_3 layer from amorphous to crystalline. ORD examination demonstrates that polarization azimuthal rotation up to ±15° can be achieved by spectrally adjustable CMDs. This work provides a new strategy to fabricate wafer-scale visible-band CMDs and further efficiently manipulate chiroptical response in an activity-adjustable manner.

METHODS

FDTD simulations. FDTD was used to calculate the chiroptical response of the CMDs. The structure model [Supplementary Fig. S9.] was built by using 3DMAX software, then it was imported into Lumerical software. The absorption response of the CMDs was calculated by the total scattered field, under the excitation of the left- and right-handed CPL. The optical parameters of Sb_2S_3 were obtained from our previous work.[27] The optical parameters of Au and Ag were taken from the experimental measurements of Johnson and Christy,[30] and the optical parameters of SiO_2 were taken from Palik handbook.[31]

ASSOCIATED CONTENT

Supporting Information

Fabrication process of CMDs with intensity, handedness and spectrum adjustability; SEM image of CMDs at low magnification; Experimental CD spectra and *g*-factor of CMDs; Experimental and calculated unpolarized absorption spectra of CMDs; Theoretically predicted differential absorption spectra of CMDs; Enhanced optical chirality distributions of CMDs.

AUTHOR INFORMATION

Corresponding Author

Wending Zhang–Key Laboratory of Light Field Manipulation and Information Acquisition, Ministry of Industry and Information Technology, Northwestern Polytechnical University, Xi'an 710129, China

E-mail: zhangwd@nwpu.edu.cn

Ting Mei-Key Laboratory of Light Field Manipulation and Information Acquisition, Ministry of Industry and Information Technology, Northwestern Polytechnical University, Xi'an 710129, China

E-mail: tmei@nwpu.edu.cn

Author

Lu Zhang-Key Laboratory of Light Field Manipulation and Information Acquisition, Ministry of Industry and Information Technology, Northwestern Polytechnical University, Xi'an 710129, China

Kun Gao-Key Laboratory of Light Field Manipulation and Information Acquisition, Ministry of Industry and Information Technology, Northwestern Polytechnical University, Xi'an 710129, China

Fanfan Lu-Key Laboratory of Light Field Manipulation and Information Acquisition, Ministry of Industry and Information Technology, Northwestern Polytechnical University, Xi'an 710129, China

Lei Xu-Advanced Optics & Photonics Laboratory, Nottingham Trent University, Nottingham NG11 8NS, United Kingdom

Mohsen Rahmani-Advanced Optics & Photonics Laboratory, Nottingham Trent University, Nottingham NG11 8NS, United Kingdom

Lixun Sun-Key Laboratory of Light Field Manipulation and Information Acquisition, Ministry of Industry and Information Technology, Northwestern Polytechnical University, Xi'an 710129, China

Feng Gao - MOE Key Laboratory of Weak-Light Nonlinear Photonics, Nankai University, Tianjin 300457

Author Contributions

W.D.Z conceived the concept and experiment, and supervised the theoretical analysis and simulations; L.Z., K.G. performed the sample preparation and optical measurements. L.Z. performed theory calculations. F.F.L., F.G., L.X.S. L.X., and M.R. analyzed the data and interpreted the results. W.D.Z. and T.M. wrote the manuscript with input from all the authors.

Notes

The authors declare no competing financial interest.

ACKNOWLEDGMENT

This work was supported by National Natural Science Foundation of China (91950207, 11974282, 12174310). Doctoral Dissertation Innovation Fund of Northwestern Polytechnical University (CX2021039). Fundamental Research Funds for Central Universities (3102019JC008).

REFERENCES

(1) Navea, S.; de Juan; & Tauler, A. R. Detection and resolution of intermediate species in protein folding processes using fluorescence and circular dichroism spectroscopies and multivariate curve resolution. *Anal. Chem.* **2002**, 74, 6031–6039.

(2) Gansel, J.; Thiel, M.; Rill, M.; Decker, M.; Bade, K.; Saile, V.; Freymann, G.; Linden, S.; Wegener, M. Gold helix photonic metamaterial as broadband circular polarizer. *Science* **2009**, 325, 1513–1515.

(3) Rodrigues, S.; Cui, Y.; Lan, S.; Kang, L.; Cai, W. Metamaterials enable chiral-selective enhancement of two-photon luminescence from quantum emitters. *Adv. Mater.* **2015**, 27, 1124–1130.

(4) Rodrigues, S.; Lan, S.; Kang, L.; Cui, Y.; Cai, W. Nonlinear imaging and spectroscopy of chiral

metamaterials. *Adv. Mater.* **2014**, 26, 6157–6162.

(5) Jansat, S.; Go´mez, M.; Philippot, K.; Muller, G.; Guiu, E.; Claver, C.; Castillón, S.; Chaudret, B. A case for enantioselective allylic alkylation catalyzed by palladium nanoparticles. *J. Am. Chem. Soc.* **2004**, 126, 1592–1593.

(6) Kang, L.; Wang, C.; Guo, X.; Ni, X.; Liu, Z.; Werner, D. Nonlinear chiral meta-mirrors: enabling technology for ultrafast switching of light polarization. *Nano Lett.* **2020**, 20, 2047−2055.

(7) Zhang, S.; Zhou, J.; Park, Y.; Rho, J.; Singh, R.; Nam, S.; Azad, A.; Chen, H.; Yin, X.; Taylor, A.; Zhang, X. Photoinduced handedness switching in terahertz chiral metamolecules. *Nat. Commun.* **2012**, 3, 942.

(8) Kan, T.; Isozaki, A.; Kanda, N.; Nemoto, N.; Konishi, K.; Takahashi, H.; Kuwata-Gonokami, M.; Matsumoto, K.; Shimoyama, I. Enantiomeric switching of chiral metamaterial for terahertz polarization modulation employing vertically deformable MEMS spirals. *Nat. Commun.* **2015**, 6, 8422.

(9) Yin, X.; Schäferling, M.; Michel, A.; Tittl, A.; Wuttig, M.; Taubner, T.; Giessen, H. Active chiral plasmonics. *Nano Lett.* **2015**, 15, 4255-4260.

(10) Chen, S.; Liu, Z.; Du, H.; Tang, C.; Ji, C.; Quan, B.; Pan, R.; Yang, L.; Li, X.; Gu, C.; Zhang, X.; Yao, Y.; Li, J.; Fang, N.; Li, J. Electromechanically reconfigurable optical nano-kirigami. *Nat. Commun.* **2021**, 12, 1299.

(11) Kuzyk, A.; Schreiber, R.; Zhang, H.; Govorov, A.; Liedl, T.; Liu, N. Reconfigurable 3D plasmonic metamolecules. *Nat. Mater.* **2014**, 13, 862-866.

(12) Nguyen, M.; Kuzyk, A. Reconfigurable chiral plasmonics beyond single chiral centers. *ACS Nano.* **2019**, 13, 13615-13619.

(13) Li, J.; Wang, M.; Wu, Z.; Li, H.; Hu, G.; Jiang, T.; Guo, J.; Liu, Y.; Yao, K.; Chen, Z.; Fang,

J.; Fan, D.; Korgel, B.; Alù, A.; Zheng, Y. Tunable chiral optics in all-solid-phase reconfigurable dielectric nanostructures. *Nano Lett.* **2021**, 21, 973-979.

(14) Lin, L.; Lepeshov, S.; Krasnok, A.; Jiang, T.; Peng, X.; Korgel, B.; Alù, A.; Zheng, Y. All-optical reconfigurable chiral meta-molecules. *Mater. Today* **2019**, 25, 10.

(15) Martens, K.; Binkowski, F.; Nguyen, L.; Hu, L.; Govorov, A.; Burger, S.; Lied, T. Long- and short-ranged chiral interactions in DNA-assembled plasmonic chains. *Nat. Commun.* **2021**, 12, 2025.

(16) Morisawa, K.; Ishida, T.; Tatsuma, T. Photoinduced chirality switching of metal-inorganic plasmonic nanostructures. *ACS Nano* **2020**, 14, 3603-3609.

(17) Saito, K.; Tatsuma, T. Chiral plasmonic nanostructures fabricated by circularly polarized light. *Nano Lett.* **2018**, 18, 3209-3212.

(18) Gao, P.; He, J.; Zhou, S.; Yang, X.; Li, S.; Sheng, J.; Wang, D.; Yu, T.; Ye, J.; Cui, Y. Large-area nanosphere self-assembly by a micropropulsive injection method for high throughput periodic surface nanotexturing. *Nano Lett.* **2015**, 15, 4591–4598.

(19) Hsu, C.; Connor, S.; Tang, X.; Cui, Y. Wafer-scale silicon nanopillars and nanocones by Langmuir-Blodgett assembly and etching. *Appl. Phys. Lett.* **2008**, 93, 133109.

(20) Hou, Y.; Leung, H.; Chan, C.; Du, J.; Chan, H.; Lei, D. Ultrabroadband Optical Superchirality in a 3D Stacked-Patch Plasmonic Metamaterial Designed by Two-Step Glancing Angle Deposition. *Adv. Funct. Mater.* **2016**, 26, 7807–7816.

(21) Wang, Z.; Ai, B.; Zhou,Z.; Guan, Y.; Möhwald, H.; Zhang, G. Free-Standing Plasmonic Chiral Metamaterials with 3D Resonance Cavities, *ACS Nano* **2018**, 12, 10914−10923.

(22) Liu, S.; Liu, J.; Cao, Z.; Fan, J.; D. Lei. Dynamic tuning of enhanced intrinsic circular ichroism in plasmonic stereo-metamolecule array with surface lattice resonance. *Nanophotonics*

2020, 9, 3419–3434.

(23) Wang, G.; Hao, C.; Ma, W.; Qu, A.; Chen, C.; Xu, J.; Xu, C.; Kuang, H.; Xu, L. Chiral plasmonic triangular nanorings with sers activity for ultrasensitive detection of amyloid proteins in alzheimer's disease. *Adv. Mater.* **2021**, 33, 2102337.

(24) H. E. Lee, H. Y. Ahn, J. M, Y. Y. Lee, M. Kim, N. H. Cho, K. Chang, W. S. Kim, J. Rho, and K. T. Nam, Amino-acid- and peptide-directed synthesis of chiral plasmonic gold nanoparticles, Nature, **2018**, 556, 360-365.

(25) Zhang, M.; Pacheco-Peña, V.; Yu, Y.; Chen, W.; Greybush, N.; Stein, A.; Engheta, N.; Murray, C.; Kagan, C. Nanoimprinted chiral plasmonic substrates with three-dimensional nanostructures. *Nano Lett.* **2018**, 18, 7389−7394.

(26) Grahn, P.; Shevchenko, A.; Kaivola, M. Electromagnetic multipole theory for optical nanomaterials, *New J. Phys.* **2012**, 14, 093033.

(27) Gao, K.; Du, K.; Tian, S.; Wang, H.; Zhang, L.; Guo, Y.; Luo, B.; Zhang, W.; Mei, T. Intermediate phase-change states with improved cycling durability of Sb_2S_3 by femtosecond multi-pulse laser irradiation. *Adv. Funct. Mater.* **2021**, 31, 2103327.

(28) Tang, Y.; Cohen, A. Optical chirality and its interaction with matter, *Phys. Rev. Lett.* **2010**, 104, 163901.

(29) Lu, L.; Dong, W.; Behera, J.; Chew, L.; Simpson, R. Inter-diffusion of plasmonic metals and phase change materials, *J. Mater. Sci.* **2019**, 54, 2814–2823.

(30) Johnson, P.; Christy, R. Optical constants of the noble metals, *Phys. Rev. B* **1972**, 6, 4370–4379.

(31) Palik, E. D.; Gallium Arsenide (gaas), *Handbook of Optical Constants of Solids* **1985**, 1, 429−443.

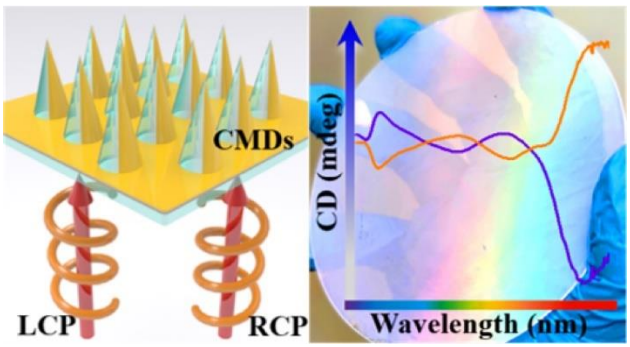

TOC graphic